

A direct comparison of single grain and multiple grain aliquot luminescence dating of feldspars from colluvial deposits in KwaZulu-Natal, South Africa

Svenja Riedesel^{1,2}, Guillaume Guérin³, Kristina J. Thomsen¹, Mariana Sontag-González⁴, Matthias Blessing^{5,6}, Greg A. Botha⁷, Max Hellers⁸, Gunther Möller⁵, Andreas Peffeköver², Christian Sommer^{9,10}, Anja Zander², Manuel Will⁵

¹Radiation Physics Division, Department of Physics, Technical University of Denmark, Roskilde/Lyngby, Denmark

²Institute of Geography, University of Cologne, Cologne, Germany

³Géosciences Rennes, UMR 6118, CNRS, Bâtiment 15, Campus Beaulieu, Université de Rennes 1, 35042 Rennes, France

⁴Institute of Geography, Justus-Liebig-Universität Giessen, D-35390 Gießen, Germany

⁵Department of Early Prehistory and Quaternary Ecology, University of Tübingen, 72070 Tübingen, Germany

⁶Deep History Lab, Department of Anthropology, University of Connecticut, Storrs, CT, USA

⁷Geological Sciences, School of Agricultural, Earth and Environmental Sciences, University of KwaZulu-Natal, Westville, South Africa

⁸Institute of Geology and Mineralogy, University of Cologne, Cologne, Germany

⁹Institute of Geography, Department of Geosciences, University of Tübingen

¹⁰The Role of Culture in Early Expansions of Humans, Heidelberg Academy of Sciences and Humanities, Tübingen, Germany

¹¹Palaeo-Research Institute, University of Johannesburg, P.O. Box 524, Auckland Park ZA-2006, Johannesburg, South Africa

Correspondence to: Svenja Riedesel (riedeselsvenja@gmail.com)

Supplementary Material

This supplementary material provides additional information on the performed luminescence measurements and respective results, as well as further insights into the determination of internal K content and the nature of the samples. The supplementary material is divided in two sections: (1) Sample characterisation and dose rate determination and (2) Protocol determination and equivalent dose measurements.

List of contents

Section 1 – Sample characterisation and dose rate determination

Fig. S1 – Single grain K₂O contents and electron backscatter images

Table S1a – Single grain K₂O contents sample JOJO-1-2

Table S1b – Single grain K₂O contents sample JOJO-5-4

Fig. S2 – Thin sections of source rock (dolerite)

Section 2 – Protocol determination and equivalent dose measurements

Table S2 – Preheat and stimulation temperature combinations tested

Fig. S3 – Dose-recovery ratios (residual subtracted) and fading rates

Fig. S4 – Examples of multi-grain aliquot luminescence signals

Fig. S5 – Examples of single grain luminescence signals

Fig. S6 – Single grain equivalent dose distributions of dose recovery tests

Fig. S7 – Sample and data-set dependent D₀ values and dose-response curves

Fig. S8 – *Sigma m* in the Average Dose Model

Fig. S9 – BayLum MCMC trajectories for JOJO-1-1

Fig. S10 – Comparison of MG- aliquots post-IR IRSL₂₂₅ ages and MG fading corrected IRSL₅₀ ages

Fig. S11 – LS-normalisation results for single grains

Fig. S12 – LS-normalisation results for multi-grain aliquots

Fig. S13 – Evaluation of the SGC L_nT_n approach

Section 1 - Sample characterisation and dose rate determination

Internal K₂O-concentrations of individual grains were determined using a JEOL JXA-8900RL Electron Microprobe. Analyses were conducted with an accelerating voltage of 15 kV, a beam current of 20 nA and a beam diameter of 4 μm. All elements were calibrated with mineral reference materials and matrix-matched reference materials were analysed for quality-control. Counting times on peak and on background were 30 s for Mg, Fe, Ti, Mn, and Ba, 20 s for Si, Al, Ca, and K, and 10 s for Na. The ZAF method was applied for matrix correction, which includes the correction for the atomic number effect (Z), the absorption effect (A), and the fluorescence excitation effect (F).

Measurement results of the 46 grains are given in Table S1a and b and are illustrated in Fig. S1a. The grains were selected to represent a range of non-luminescent, as well as IRSL₅₀, post-IRIRSL₂₂₅ and both signals emitting grains. Due to the intense weathering of the grains, not all grains present on the discs could be measured, because insufficiently large mineral areas were present for the spot size of the electron beam.

Furthermore, electron backscatter images of four selected grains are shown in Fig. S1b-e. The mineral phases indicated in these sub-figures were identified by EDS (energy-dispersive x-ray spectroscopy). These electron backscatter images reveal the highly weathered condition of the grains, with large parts of the feldspar grains already replaced by clay minerals. This weathering is also visible in the polarised microscope photographs of the source rock in Fig. S2a and S2b. Whilst the dolerite sample displayed in Fig. S2a was chipped off from a non-exposed rock surface, the piece of rock shown in Fig. S2b was taken from the weathered and exposed rock surface. Weathering along cracks in the rocks is visible from the brownish areas in Fig. S2b.

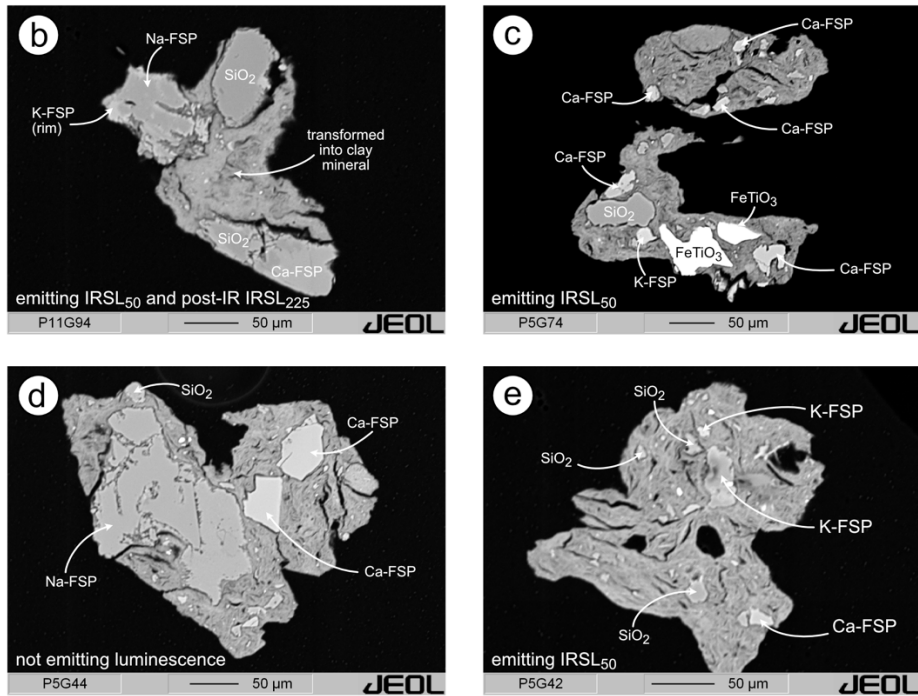
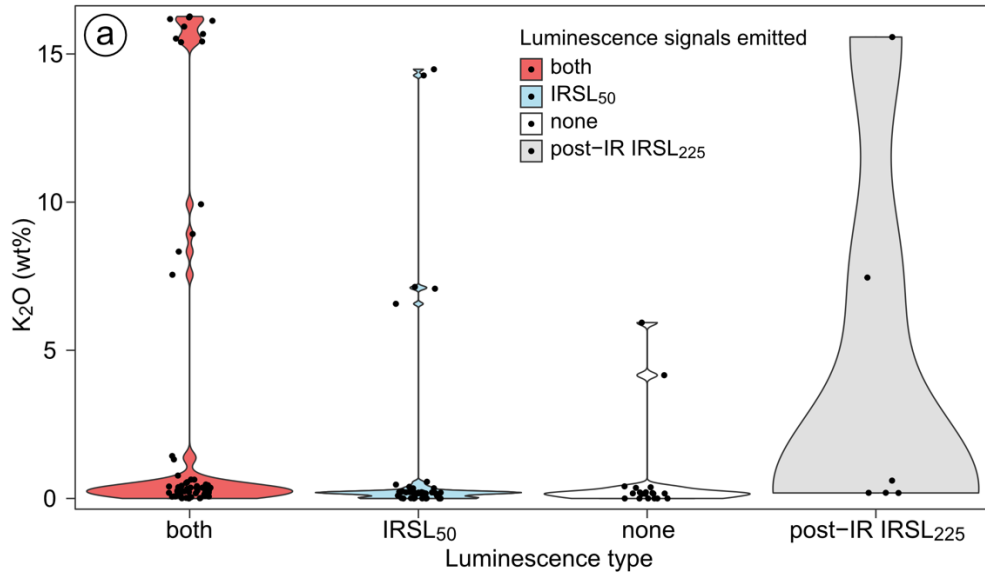


Fig. S1. a) Results of the chemical composition of individual grains determined using wavelength dispersive x-ray spectroscopy. In total 44 grains were measured, out of those grains 19 emitted IRSL₅₀ and post-IR IRSL₂₂₅, 16 only IRSL₅₀, 2 only post-IR IRSL₂₂₅ and 7 did not emit any luminescence. Two or three points were measured per grain and the distribution of individual measurements are shown as violin plots with individual data points displayed in the figure. B-e) Electron back scatter images of four selected grains. The mineralogical composition indicated on the images is based on EDS analysis performed using an electron microprobe. The images show the intense weathering of the grains, with large parts of the grains already transformed into clay minerals. The phase indicated as ‘SiO₂’ represents an alteration product of feldspar after extensive leaching. Based on the EDS measurements, the backscatter images and the source rock type (dolerite), the original grains will have been plagioclases, with a few exceptions, also containing K₂O.

Table S1a. Results of electron microprobe analysis for the 30 grains selected from sample JOJO-1-2. The uncertainties the standard error of all measurements performed on the individual grains, with two to six points measured on each grain. Results are given in wt%.

| Sample ID | Lum. | n | MgO | FeO | Na ₂ O | K ₂ O | TiO ₂ | SiO ₂ | MnO | Al ₂ O ₃ | CaO | BaO | Total |
|-----------------|--------------------------------|---|-------------|-------------|-------------------|------------------|------------------|------------------|-------------|--------------------------------|--------------|-------------|---------------|
| JOJO-1-2 P1 G10 | none | 3 | 0.04 ± 0.01 | 0.75 ± 0.01 | 6.04 ± 0.12 | 0.38 ± 0.01 | 0.07 ± 0.01 | 56.56 ± 0.23 | 0 ± 0 | 27.62 ± 0.12 | 9.76 ± 0.12 | 0.05 ± 0.02 | 101.26 ± 0.21 |
| JOJO-1-2 P1 G1 | none | 3 | 0.07 ± 0.01 | 0.62 ± 0.04 | 3.97 ± 0.04 | 0.17 ± 0.01 | 0.06 ± 0 | 51.25 ± 0.03 | 0.02 ± 0.01 | 30.46 ± 0.09 | 13.29 ± 0.06 | 0.02 ± 0.01 | 99.94 ± 0.16 |
| JOJO-1-2 P1 G11 | none | 2 | 0.13 ± 0 | 0.7 ± 0.03 | 4.13 ± 0.07 | 0.21 ± 0 | 0.06 ± 0 | 53.36 ± 0.21 | 0 ± 0 | 30.94 ± 0.04 | 13.3 ± 0.06 | 0.02 ± 0.02 | 102.84 ± 0.4 |
| JOJO-1-2 P1 G20 | IRSL ₅₀ | 1 | 0.08 | 0.59 | 3.67 | 0.17 | 0.06 | 50.37 | 0.00 | 28.57 | 12.36 | 0.01 | 95.88 |
| JOJO-1-2 P1 G29 | IRSL ₅₀ | 3 | 0.17 ± 0.08 | 1.15 ± 0.51 | 4.18 ± 0.31 | 0.2 ± 0 | 0.11 ± 0.01 | 56.46 ± 2.19 | 0.02 ± 0 | 28.16 ± 1.16 | 11.28 ± 0.97 | 0.02 ± 0.01 | 101.75 ± 0.6 |
| JOJO-1-2 P1 G28 | IRSL ₅₀ | 1 | 0.03 | 0.31 | 0.00 | 0.02 | 0.03 | 101.14 | 0.00 | 0.16 | 0.01 | 0.00 | 101.69 |
| JOJO-1-2 P1 G49 | both | 5 | 0 ± 0 | 0.06 ± 0.03 | 1.02 ± 0.92 | 2.45 ± 1.89 | 0.16 ± 0.02 | 90.99 ± 6.39 | 0.02 ± 0.01 | 4.62 ± 3.67 | 0.09 ± 0.07 | 0.05 ± 0.04 | 99.47 ± 0.21 |
| JOJO-1-2 P3 G10 | none | 3 | 0.07 ± 0.04 | 0.75 ± 0.12 | 3.23 ± 0.39 | 3.42 ± 1.7 | 0.38 ± 0.17 | 71.27 ± 9.39 | 0.04 ± 0.02 | 17.97 ± 7.06 | 4.92 ± 4.53 | 0.08 ± 0.03 | 102.14 ± 1.02 |
| JOJO-1-2 pP3 G8 | none | 3 | 0 ± 0 | 0.03 ± 0 | 0.02 ± 0.01 | 0 ± 0 | 0.1 ± 0.01 | 97.84 ± 0.13 | 0.01 ± 0.01 | 0.11 ± 0.02 | 0.01 ± 0 | 0.02 ± 0.01 | 98.16 ± 0.13 |
| JOJO-1-2 P3 G7 | IRSL ₅₀ | 3 | 0 ± 0 | 0.29 ± 0.02 | 2.63 ± 0.37 | 6.93 ± 0.18 | 0.1 ± 0.02 | 78.25 ± 1.05 | 0.03 ± 0.01 | 11.74 ± 0.45 | 0.07 ± 0.02 | 0.06 ± 0.01 | 100.09 ± 0.3 |
| JOJO-1-2 P3 G5 | none | 3 | 0.01 ± 0 | 0.09 ± 0.01 | 0 ± 0 | 0 ± 0 | 0.08 ± 0.01 | 96.77 ± 0.09 | 0 ± 0 | 0.07 ± 0.02 | 0 ± 0 | 0.01 ± 0 | 97.02 ± 0.09 |
| JOJO-1-2 P3 G2 | IRSL ₅₀ | 3 | 0 ± 0 | 0.16 ± 0.02 | 5.59 ± 1.14 | 0.32 ± 0.14 | 0.15 ± 0.03 | 80.69 ± 1.88 | 0.02 ± 0.01 | 11.67 ± 1.52 | 1.37 ± 0.23 | 0.05 ± 0 | 100.01 ± 0.55 |
| JOJO-1-2 P3 G13 | IRSL ₅₀ | 4 | 0 ± 0 | 0.26 ± 0.11 | 0.11 ± 0.03 | 0.05 ± 0.02 | 0.05 ± 0.02 | 97.04 ± 0.42 | 0.01 ± 0.01 | 0.42 ± 0.05 | 0.01 ± 0 | 0.02 ± 0.01 | 97.97 ± 0.32 |
| JOJO-1-2 P3 G39 | IRSL ₅₀ | 3 | 0.01 ± 0.01 | 0.57 ± 0.1 | 8.87 ± 2.2 | 0.37 ± 0.02 | 0.1 ± 0.02 | 63.61 ± 6.16 | 0.01 ± 0.01 | 23.04 ± 3.81 | 4.66 ± 4.11 | 0.01 ± 0 | 101.24 ± 0.31 |
| JOJO-1-2 P3 G37 | both | 1 | 0.07 | 0.54 | 4.48 | 0.20 | 0.05 | 52.93 | 0.00 | 29.46 | 12.25 | 0.01 | 99.99 |
| JOJO-1-2 P3 G50 | both | 4 | 0.05 ± 0.01 | 0.73 ± 0.03 | 4.48 ± 0.44 | 0.22 ± 0.03 | 0.06 ± 0.01 | 52.21 ± 0.95 | 0.02 ± 0.01 | 29.7 ± 0.67 | 12.43 ± 0.77 | 0.01 ± 0.01 | 99.9 ± 0.09 |
| JOJO-1-2 P3 G60 | both | 1 | 0.00 | 0.31 | 0.01 | 0.01 | 0.12 | 99.91 | 0.00 | 0.08 | 0.00 | 0.05 | 100.49 |
| JOJO-1-3 P3 G70 | both | 5 | 0 ± 0 | 0.12 ± 0.03 | 0.98 ± 0.47 | 4.98 ± 2.03 | 0.22 ± 0.15 | 85.23 ± 5.24 | 0.02 ± 0.01 | 7.26 ± 2.87 | 0.23 ± 0.16 | 0.07 ± 0.02 | 99.11 ± 0.31 |
| JOJO-1-2 P3 G54 | post-IR IRSL ₂₂₅ | 1 | 0.06 | 0.71 | 4.32 | 0.19 | 0.05 | 52.05 | 0.00 | 30.10 | 12.70 | 0.00 | 100.17 |
| JOJO-1-2 P5 G9 | IRSL ₅₀ | 1 | 0.09 | 0.56 | 4.39 | 0.22 | 0.08 | 51.29 | 0.00 | 28.43 | 12.08 | 0.01 | 97.14 |
| JOJO-1-2 P5 G19 | IRSL ₅₀ | 3 | 0.07 ± 0 | 0.78 ± 0.01 | 4.66 ± 0.26 | 0.2 ± 0.02 | 0.11 ± 0.01 | 51.06 ± 0.73 | 0.01 ± 0.01 | 28.4 ± 0.36 | 11.96 ± 0.51 | 0.04 ± 0.01 | 97.3 ± 0.14 |
| JOJO-1-2 P5 G16 | both | 3 | 0.01 ± 0.01 | 0.6 ± 0.06 | 8.17 ± 0.82 | 0.42 ± 0.05 | 0.06 ± 0.01 | 60.26 ± 1.61 | 0.01 ± 0.01 | 24.15 ± 1.15 | 6 ± 1.32 | 0.04 ± 0.03 | 99.73 ± 0.17 |
| JOJO-1-2 P5 G14 | IRSL ₅₀ | 3 | 0.02 ± 0.01 | 0.07 ± 0.02 | 2.45 ± 2.44 | 0.04 ± 0.03 | 0.07 ± 0.04 | 91.44 ± 5.59 | 0.01 ± 0 | 3.87 ± 3.79 | 0.05 ± 0.05 | 0.02 ± 0.01 | 98.03 ± 0.73 |
| JOJO-1-2 P5 G30 | IRSL ₅₀ | 3 | 0.05 ± 0.01 | 0.93 ± 0.06 | 4.27 ± 0.2 | 0.23 ± 0.02 | 0.07 ± 0.01 | 51.93 ± 0.37 | 0 ± 0 | 29.56 ± 0.15 | 12.72 ± 0.25 | 0.04 ± 0.02 | 99.8 ± 0.43 |
| JOJO-1-2 P5 G99 | both | 3 | 0.03 ± 0 | 0.92 ± 0.07 | 4.83 ± 0.07 | 0.29 ± 0.01 | 0.07 ± 0 | 53.76 ± 0.15 | 0.01 ± 0.01 | 29.15 ± 0.16 | 11.77 ± 0.13 | 0.01 ± 0 | 100.84 ± 0.18 |
| JOJO-1-2 P5 G98 | none | 3 | 0.09 ± 0.01 | 0.65 ± 0.02 | 3.9 ± 0.02 | 0.16 ± 0 | 0.06 ± 0.01 | 51.17 ± 0.18 | 0.01 ± 0.01 | 30.16 ± 0.04 | 13.4 ± 0.02 | 0.01 ± 0.01 | 99.61 ± 0.18 |
| JOJO-1-2 P5 G44 | IRSL ₅₀ | 7 | 0.05 ± 0.02 | 0.51 ± 0.14 | 4.04 ± 1.45 | 0.13 ± 0.03 | 0.07 ± 0.01 | 67.36 ± 8.47 | 0 ± 0 | 19.52 ± 5.21 | 7.38 ± 2.58 | 0.01 ± 0 | 99.06 ± 0.29 |
| JOJO-1-2 P5 G74 | post-IR IRSL ₂₂₅ | 5 | 0.05 ± 0.02 | 0.57 ± 0.08 | 4.15 ± 1.14 | 4.8 ± 3.03 | 0.1 ± 0.01 | 58.33 ± 2.72 | 0.01 ± 0 | 23.31 ± 3.1 | 6.4 ± 2.87 | 0.12 ± 0.07 | 97.84 ± 1.61 |
| JOJO-1-2 P5 G66 | both | 4 | 0.04 ± 0.02 | 0.52 ± 0.18 | 2.44 ± 0.84 | 7.8 ± 4.4 | 0.02 ± 0.01 | 57.64 ± 3.59 | 0.01 ± 0.01 | 24.26 ± 3.31 | 6.72 ± 3.87 | 0.12 ± 0.06 | 99.55 ± 0.3 |

Table S1b. Results of electron microprobe analysis for the 16 grains selected from sample JOJO-5-4. The uncertainties the standard error of all measurements performed on the individual grains, with two to six points measured on each grain. Results are given in wt%.

| Sample ID | Lum. | n | MgO | FeO | Na ₂ O | K ₂ O | TiO ₂ | SiO ₂ | MnO | Al ₂ O ₃ | CaO | BaO | Total |
|------------------|--------------------|---|--------------|-------------|-------------------|------------------|------------------|------------------|-------------|--------------------------------|--------------|-------------|---------------|
| JOJO-5-4 P7 G91 | both | 3 | 0 ± 0 | 0.04 ± 0.02 | 0.82 ± 0.09 | 15.91 ± 0.13 | 0 ± 0 | 64.7 ± 0.15 | 0.01 ± 0.01 | 18.84 ± 0.08 | 0 ± 0 | 0.22 ± 0.01 | 100.54 ± 0.24 |
| JOJO-5-4 P7 G92 | IRSL ₅₀ | 3 | 0.05 ± 0.01 | 0.73 ± 0.03 | 3.86 ± 0.04 | 0.21 ± 0.01 | 0.04 ± 0.01 | 50.88 ± 0.07 | 0.02 ± 0.01 | 30.29 ± 0.15 | 13.57 ± 0.03 | 0.01 ± 0.01 | 99.66 ± 0.12 |
| JOJO-5-4 P7 G70 | both | 3 | 0.03 ± 0.02 | 0.48 ± 0.14 | 6.01 ± 3.26 | 0.18 ± 0.14 | 0.05 ± 0.02 | 74.6 ± 12.14 | 0 ± 0 | 15.97 ± 8.12 | 3.41 ± 2.62 | 0.03 ± 0.01 | 100.75 ± 0.88 |
| JOJO-5-4 P7 G59 | both | 3 | 0 ± 0 | 0.1 ± 0.03 | 7.91 ± 3.96 | 0.05 ± 0.03 | 0.03 ± 0.01 | 79.07 ± 9.96 | 0 ± 0 | 13.25 ± 6.61 | 0.07 ± 0.03 | 0.02 ± 0.01 | 100.51 ± 0.69 |
| JOJO-5-4 P7 G60 | IRSL ₅₀ | 3 | 0 ± 0 | 0.24 ± 0.02 | 1.48 ± 0.07 | 14.38 ± 0.1 | 0.03 ± 0 | 64.5 ± 0.04 | 0 ± 0 | 18.76 ± 0.13 | 0.04 ± 0 | 0.34 ± 0 | 99.78 ± 0.15 |
| JOJO-5-4 P7 G30 | both | 3 | 0.09 ± 0.01 | 0.95 ± 0.08 | 4.64 ± 0.33 | 0.29 ± 0.06 | 0.08 ± 0.04 | 53.49 ± 0.67 | 0.01 ± 0.01 | 28.73 ± 0.84 | 11.92 ± 0.78 | 0.02 ± 0.01 | 100.21 ± 0.97 |
| JOJO-5-4 P7 G45 | both | 3 | 0.05 ± 0.01 | 0.62 ± 0.04 | 6.07 ± 0.11 | 0.38 ± 0.03 | 0.11 ± 0 | 55.95 ± 0.21 | 0 ± 0 | 26.81 ± 0.15 | 9.39 ± 0.23 | 0.01 ± 0.01 | 99.39 ± 0.09 |
| JOJO-5-4 P11 G20 | IRSL ₅₀ | 3 | 0.08 ± 0.04 | 0.75 ± 0.03 | 4.82 ± 0.84 | 0.28 ± 0.09 | 0.05 ± 0.01 | 53.74 ± 1.89 | 0.01 ± 0.01 | 28.85 ± 1.47 | 11.63 ± 1.66 | 0.04 ± 0.03 | 100.26 ± 0.33 |
| JOJO-5-4 P11 G30 | both | 3 | 0 ± 0 | 0.11 ± 0.02 | 0.49 ± 0.03 | 16.23 ± 0.03 | 0.01 ± 0.01 | 64.38 ± 0.23 | 0.03 ± 0.02 | 18.55 ± 0.05 | 0.05 ± 0.01 | 0.09 ± 0.01 | 99.93 ± 0.24 |
| JOJO-5-4 P11 G50 | IRSL ₅₀ | 3 | 14.75 ± 8.48 | 6.54 ± 3.45 | 2.22 ± 1.26 | 0.1 ± 0.06 | 0.16 ± 0.07 | 54.1 ± 0.72 | 0.11 ± 0.06 | 15.59 ± 8.26 | 7.29 ± 3.08 | 0.02 ± 0.01 | 100.86 ± 0.19 |
| JOJO-5-4 P11 G65 | both | 2 | 0.06 ± 0.06 | 0.65 ± 0.31 | 2.31 ± 1.9 | 7.85 ± 7.66 | 0.05 ± 0.01 | 55.34 ± 5.51 | 0 ± 0 | 21.84 ± 4.74 | 5.93 ± 5.92 | 0.18 ± 0.18 | 94.22 ± 0.41 |
| JOJO-5-4 P11 G64 | both | 3 | 0.03 ± 0.01 | 0.56 ± 0.03 | 5.86 ± 0.07 | 0.41 ± 0.03 | 0.14 ± 0.02 | 55.26 ± 0.14 | 0.01 ± 0.01 | 27.12 ± 0.11 | 9.84 ± 0.16 | 0.02 ± 0.01 | 99.26 ± 0.1 |
| JOJO-5-4 P11 G74 | both | 3 | 0.02 ± 0 | 0.43 ± 0.03 | 6.54 ± 0.66 | 0.33 ± 0.07 | 0.1 ± 0.01 | 60.83 ± 4.29 | 0.01 ± 0.01 | 24.23 ± 2.69 | 7.46 ± 1.97 | 0.05 ± 0.02 | 100.01 ± 0.28 |
| JOJO-5-4 P11 G84 | IRSL ₅₀ | 2 | 0 ± 0 | 0.11 ± 0.03 | 0.01 ± 0.01 | 0 ± 0 | 0.01 ± 0.01 | 98.77 ± 0.22 | 0.01 ± 0.01 | 0.01 ± 0 | 0 ± 0 | 0.01 ± 0.01 | 98.93 ± 0.26 |
| JOJO-5-4 P11 G85 | both | 3 | 0.01 ± 0.01 | 0.12 ± 0.06 | 3.08 ± 1.81 | 0.12 ± 0.08 | 0.16 ± 0.03 | 87.82 ± 6.65 | 0.02 ± 0.01 | 6.04 ± 3.67 | 0.66 ± 0.38 | 0.04 ± 0.02 | 98.08 ± 0.87 |
| JOJO-5-4 P11 G94 | both | 5 | 0.02 ± 0.01 | 0.3 ± 0.03 | 9.28 ± 0.73 | 0.7 ± 0.16 | 0.06 ± 0.01 | 61.87 ± 1.7 | 0 ± 0 | 21.1 ± 1.06 | 3.36 ± 1.27 | 0.06 ± 0.02 | 96.76 ± 0.4 |

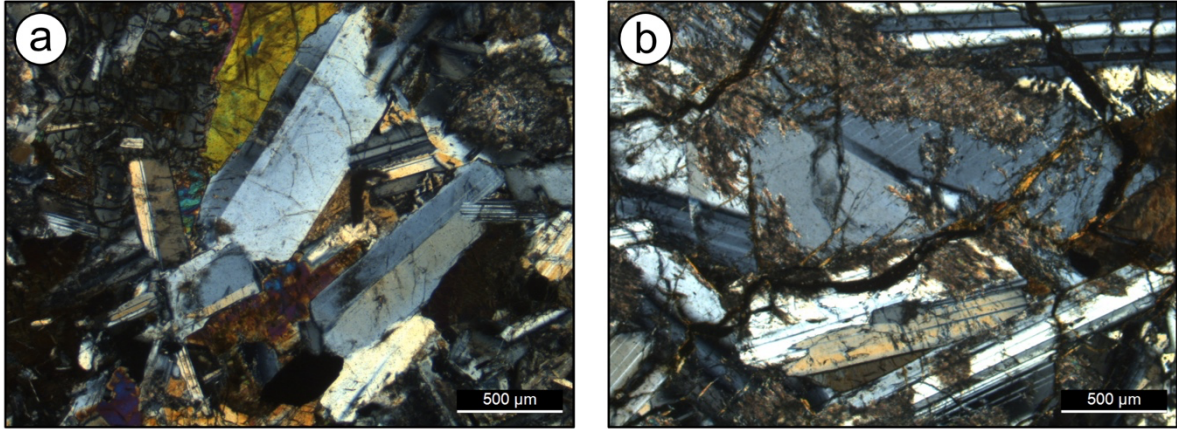


Fig. S2. A thin section of the dominant source rock in the catchment, dolerite. Under the polarised microscope plagioclase is identifiable as the major feldspar constituting to the rock mineralogy.

Section 2 – Protocol determination and equivalent dose measurements

S2.1 Protocol determination

Here we would like to give some additional information regarding the protocol selection and validation procedure, as well as some further details regarding the luminescence signals measured using the selected post-IR IRSL₂₂₅ protocol.

Table S2 shows the different preheat and stimulation temperatures tested during the protocol determination process. Whilst the protocol was first tested on multi-grain aliquots of samples JOJO-1-2 and JOJO-85U, it was validated for all samples by measuring the dose recovery ratio (Fig. S3a) of all samples, as well as fading (Fig. S3b).

Exemplary multi-grain aliquot decay curves and dose-response curves of the IRSL₅₀ and post-IR IRSL₂₂₅ signals of the selected measurement protocol are shown in Fig. S4. Single grain decay curves and dose-response curves are shown in Fig. S5.

Table S2. Preheat and post-IR IRSL stimulation temperature combinations tested in the preheat plateau tests shown in the main text's figures 2.

| Preheat temperature (°C) | First IR stimulation temperature (°C) | Post-IR IR stimulation temperature (°C) |
|--------------------------|---------------------------------------|---|
| 210 | 50 | 190 |
| 230 | 50 | 210 |
| 250 | 50 | 225 |
| 280 | 50 | 250 |
| 320 | 50 | 290 |

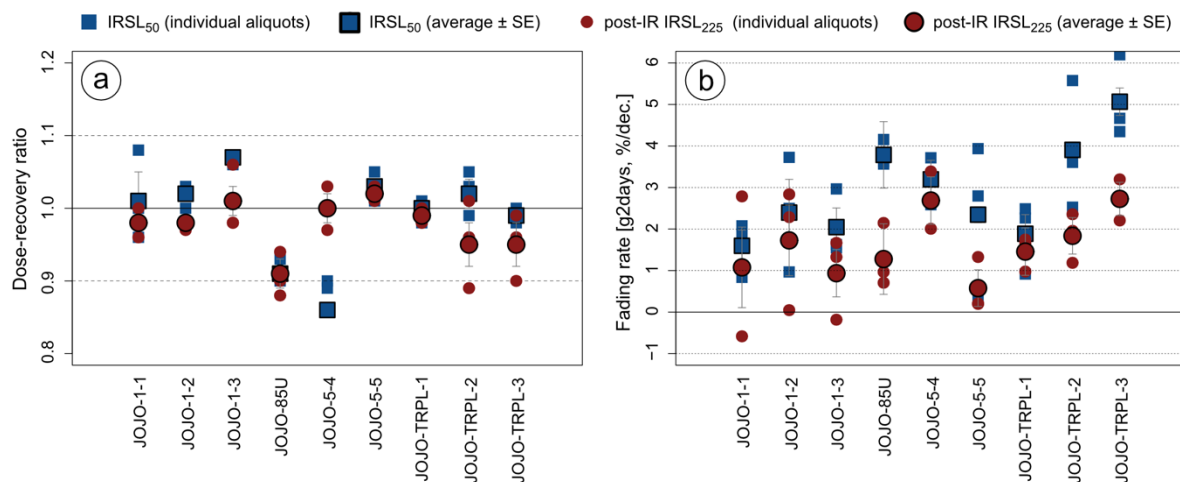


Fig. S3. (a) Dose-recovery ratios (residual subtracted) and (b) fading rates obtained for individual aliquots of all samples and calculated average values and their standard error, for IRSL₅₀ and post-IR IRSL₂₂₅ signals. Three aliquots were measured per sample using the protocol by Auclair et al. (2003).

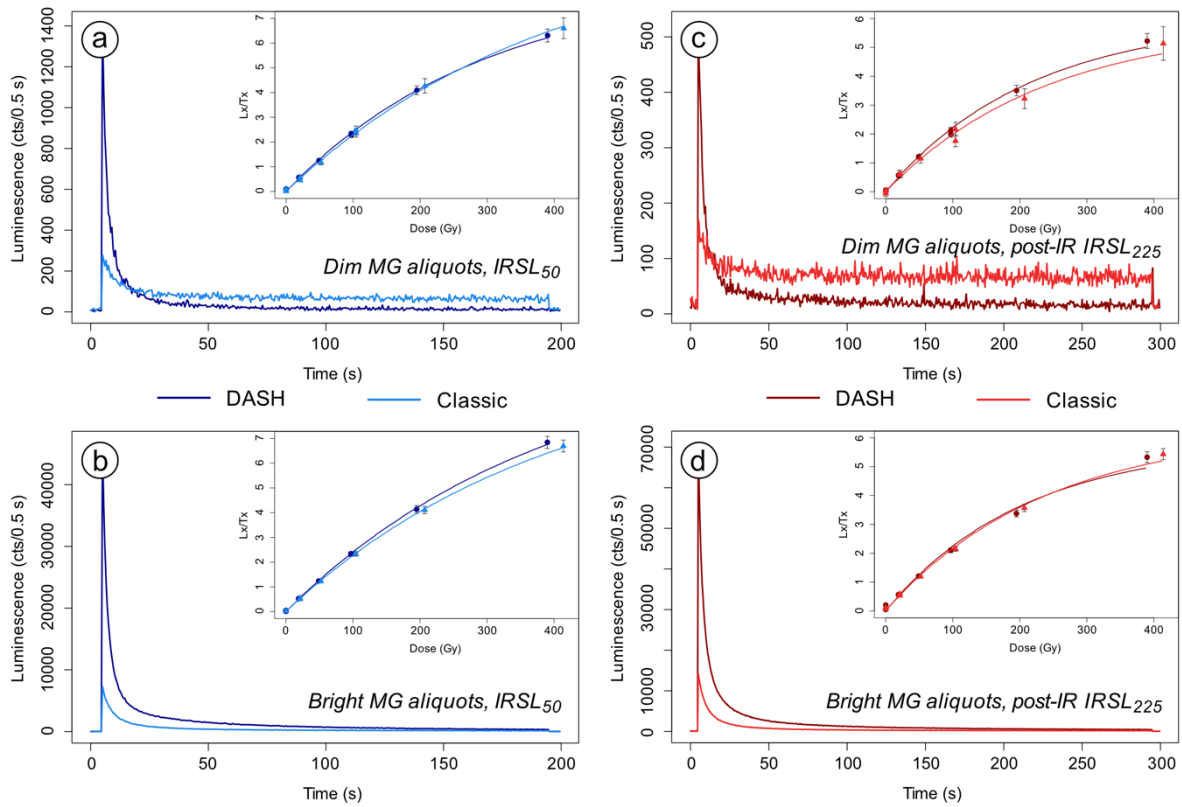


Fig. S4. Examples of “dim” and “bright” multi-grain aliquots (1 mm diameter) measured on a Risø TL/OSL DA20 with a classic head and a DASH (detection and stimulation head). These are examples of representative aliquots, this is not an absolute comparison of the same aliquots measured on different readers. (a) and (b) are the IRSL₅₀ signals and (c) and (d) the post-IR IRSL₂₂₅ signals. The insets show the dose-response curves for the respective aliquots. The decay curves were obtained in response to a dose of 100 Gy.

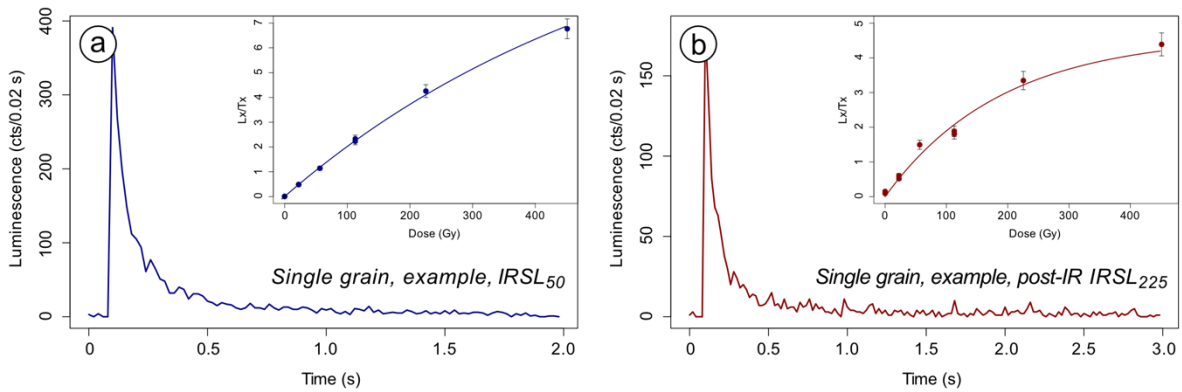


Fig. S5. Examples of single grain decay curves and dose response curves of the IRSL₅₀ and post-IR IRSL₂₂₅ signals of the selected measurement protocol. The decay curves were obtained in response to a dose of 100 Gy.

S2.2 Equivalent dose determination and palaeodose calculations

S2.2.1 Dose distributions

In Fig. S6 the single grain dose recovery dose distributions for samples JOJO-1-3 and JOJO-85U are shown. The samples were loaded in the single-grain discs, bleached in the solar simulator at room temperature for 24 h prior to dosing. The samples were both given a dose of 100 Gy.

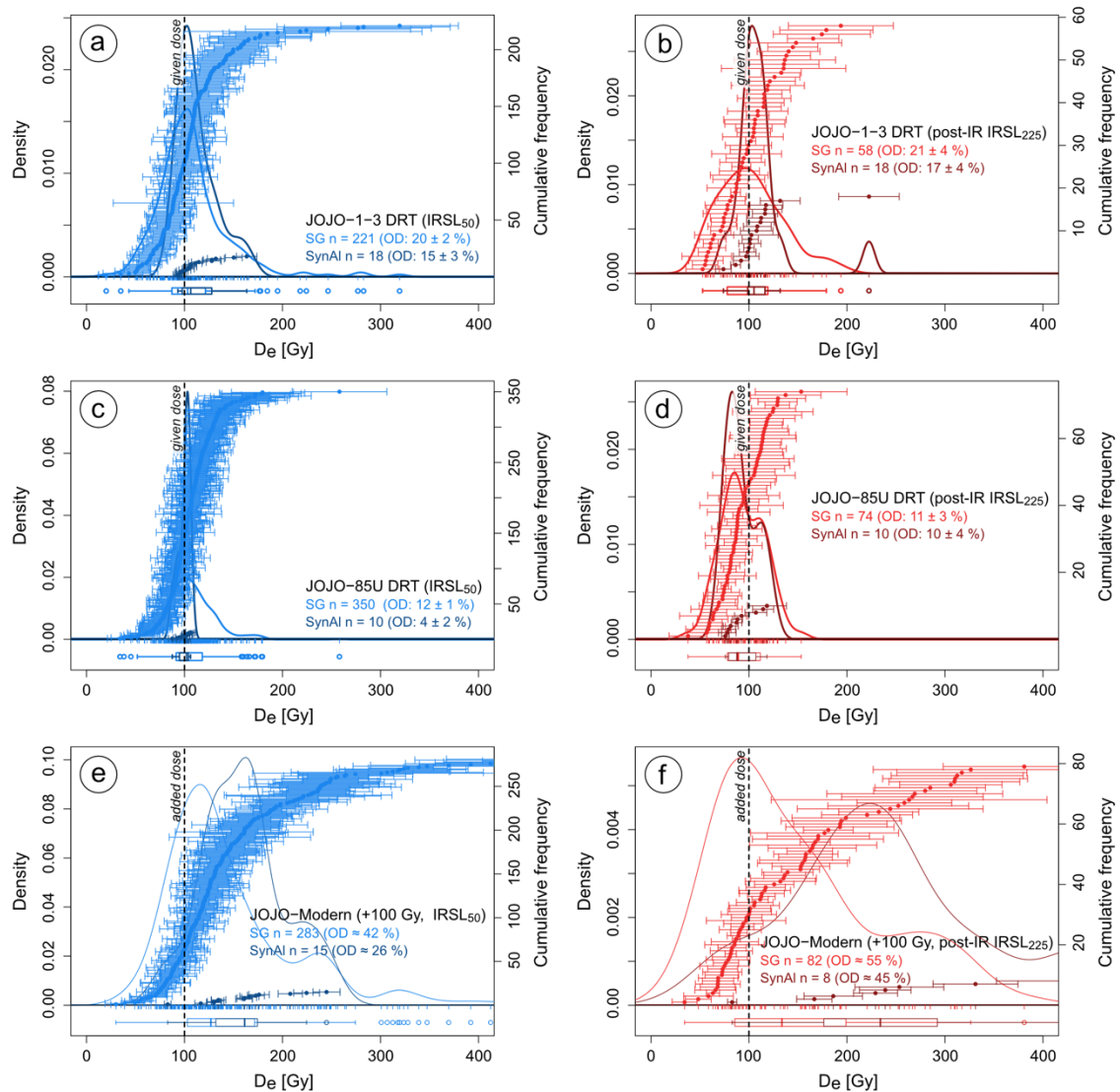


Fig. S6. Single grain dose recovery distributions for samples JOJO-1-3 (a, b) and JOJO-85U (c, d). The samples were bleached for 24 h in a solar simulator before being given a beta dose of 100 Gy. Data are shown as Kernel Density Estimate (KDE) plots for both the IRSL₅₀ (a, c) and the post-IR IRSL₂₂₅ signals (b, d).

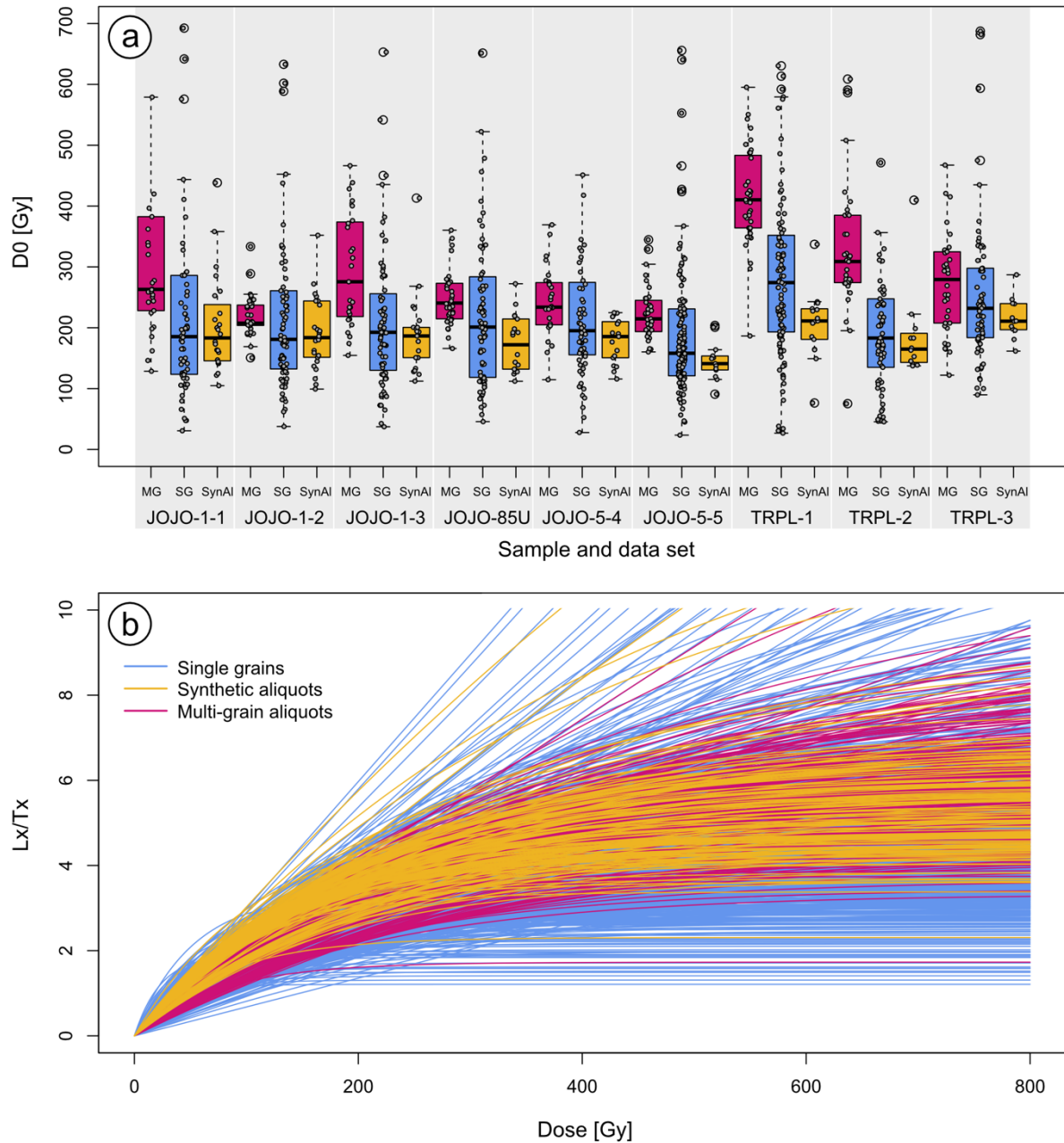


Fig. S7. Variations in D_0 (A) and dose response curve shape (B) for postIR-IRSL₂₂₅ signals from all single grains (blue), synthetic aliquots (yellow) and 1 mm aliquots (pink) accepted according to the in the main text outlined rejection criteria. Interestingly, single grains and synthetic aliquots seem to saturate earlier in case of all samples, compared to multi-grain aliquots.

Fig. S7 show D_0 values and dose response curves of all single grains, synthetic aliquots and multi-grain aliquots accepted using the in the main text applied Analyst acceptance criteria. The box plot in Fig. S7 shows large variation in D_0 for all samples. However, the median of the D_0 distributions is always below the median of the multi-grain aliquot D_0 distributions. Synthetic aliquots, in contrast, show median values consistent with the single grain data sets for most samples, except for JOJO-5-5 and JOJO-TRPL-1. The effect of the difference in D_0 value between single grains and multi-grain aliquots on the number of samples showing saturated grains and aliquots, and thus on the dose calculations is discussed in the main text.

S2.2.2 Standard frequentist approaches (Central Age Model and Average Dose Model)

Dose calculations following frequentist approaches were carried out on single grain, synthetic aliquot and multi-grain (1 mm) aliquot data. The analysis of the dose response curve as well as equivalent dose calculations were carried out using Analyst (Duller, 2015). Burial doses were calculated from obtained equivalent doses using the `calc_CentralDose()` (Burow, 2023) and `calc_AverageDose()` (Christophe et al., 2023) functions in the RLuminescence package (Kreutzer et al., 2023).

For the Central Age Model (CAM, Galbraith et al., 1999) the logged version was used. The `calc_CentralDose()` function also provided the relative overdispersion presented for each sample in the main text.

The Average Dose Model (ADM, Guérin et al., 2017) requires the input of a value for the intrinsic overdispersion (σ_m), which is generally determined from dose recovery experiments. Figure S5 shows the results of testing the influence of different σ_m values for palaeodose calculations. The results are exemplarily shown for single grains and synthetic aliquots of samples JOJO-1-3 and JOJO-5-5. The shaded areas show the overdispersion estimated from single grain dose recovery tests (at 100 Gy). From these single grain dose recovery tests, synthetic aliquots were created for each single grain disc measured and overdispersions were calculated for these data sets. Finally, the calculated overdispersion values were used for ADM calculations, with single grain dose recovery overdispersion used for single grains and synthetic aliquots overdispersions used for synthetic aliquot and multi-grain aliquot calculations.

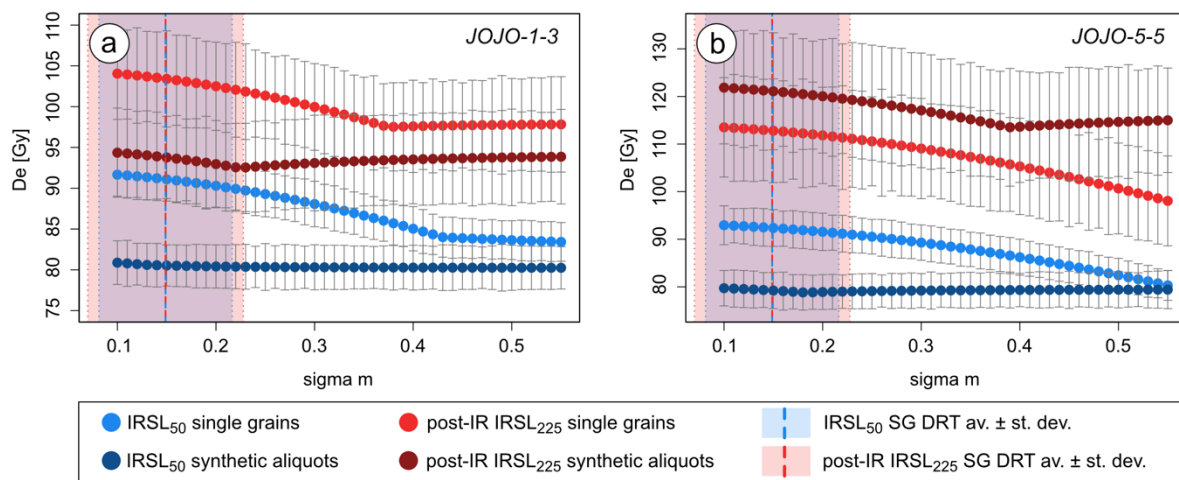


Fig. S8. Impact of changing σ_m on the D_e calculated using the ADM (a, b). Subfigure (a) shows the results for JOJO-1-3 and subfigure (b) for JOJO-5-5. The shaded areas and dashed vertical lines show the results of overdispersions estimated for laboratory single grain dose recovery tests.

S2.2.3 BayLum

BayLum was used by employing the functions available in the RPackage BayLum (Philippe et al., 2019). For this the 1 mm aliquot and single grain data sets were screened according to the acceptance criteria outlined in the main text using Analyst (Duller, 2015). However, in contrast to the frequentist approaches, for BayLum also saturated MG aliquots and single grains were considered. The .binx files, disc and grain positions of these accepted aliquots and grains were put into BayLum.

Furthermore, BayLum requires the input of the environmental dose rate and its uncertainty squared (obtained using DRAC), as well as the dose rate of the luminescence instrument used to create the respective .binx files.

The function Age_Computation() ran with PriorAge and Iter (iterations) suitable for each sample. A saturating single exponential fit was used to fit the dose response curves, and the curves were forced through the origin. A gaussian distribution was assumed for the distribution of individual doses around the palaeodose.

Prior to accepting the results, they were evaluated for proper convergence. For this the Gelman and Rubin test of convergence was performed (this is provided by BayLum) and it was assured that convergence was reached for the age, palaeodose and the equivalent dose dispersion parameters (all below 1.05, Philippe et al., 2019). Furthermore, we visually inspected the by BayLum provided plot output, which provides a mean of evaluating the MCMC trajectories (see Fig. S6 as an example).

The final ages, presented in Table 5 and Fig. 6 in the main text, were calculated using BayLum with stratigraphic control. Therefore the AgeS_Computation() function was used. All three profiles were run together, but stratigraphic information (indicating dependencies in depth, i.e. above or below a certain sample) was only used within a certain profile.

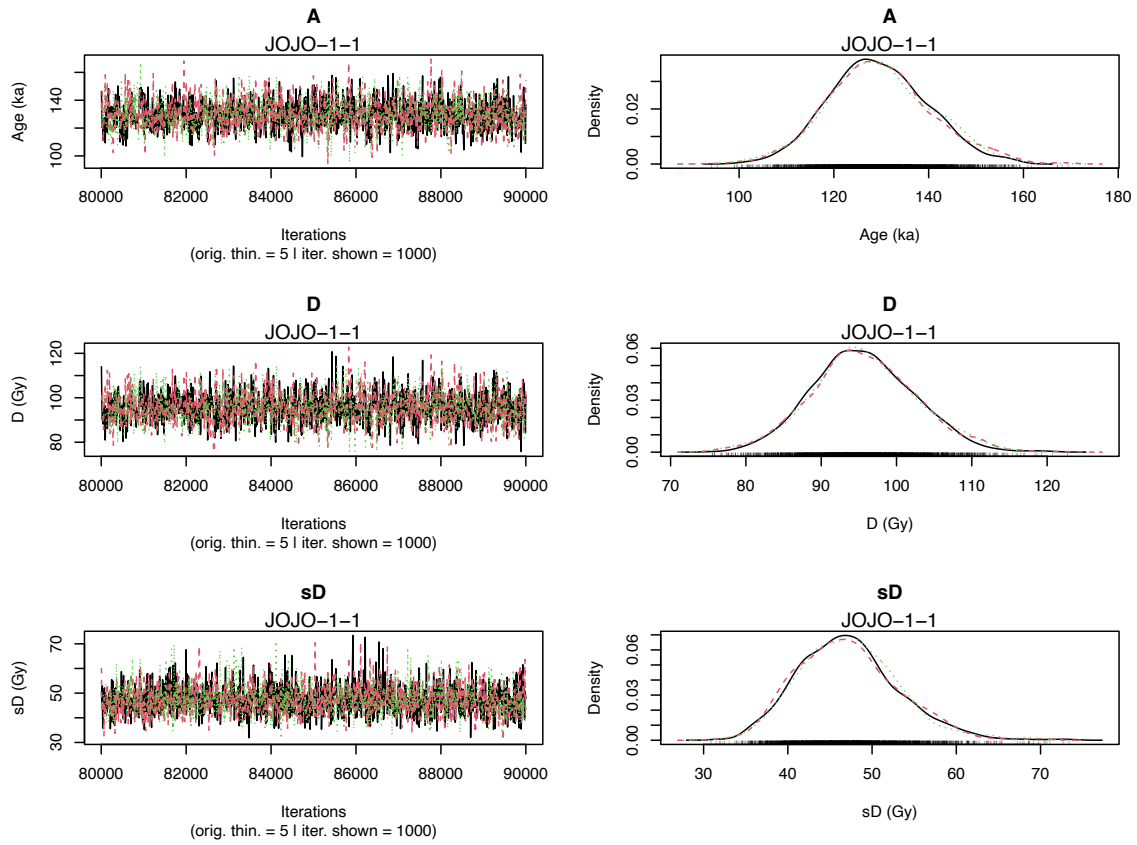


Fig. S9 BayLum MCMC trajectories for the age (A), palaeodose (D) and equivalent dose dispersion (sD) used for assessing the quality of the BayLum results, here exemplarily shown for the single grain data set of JOJO-1-1.

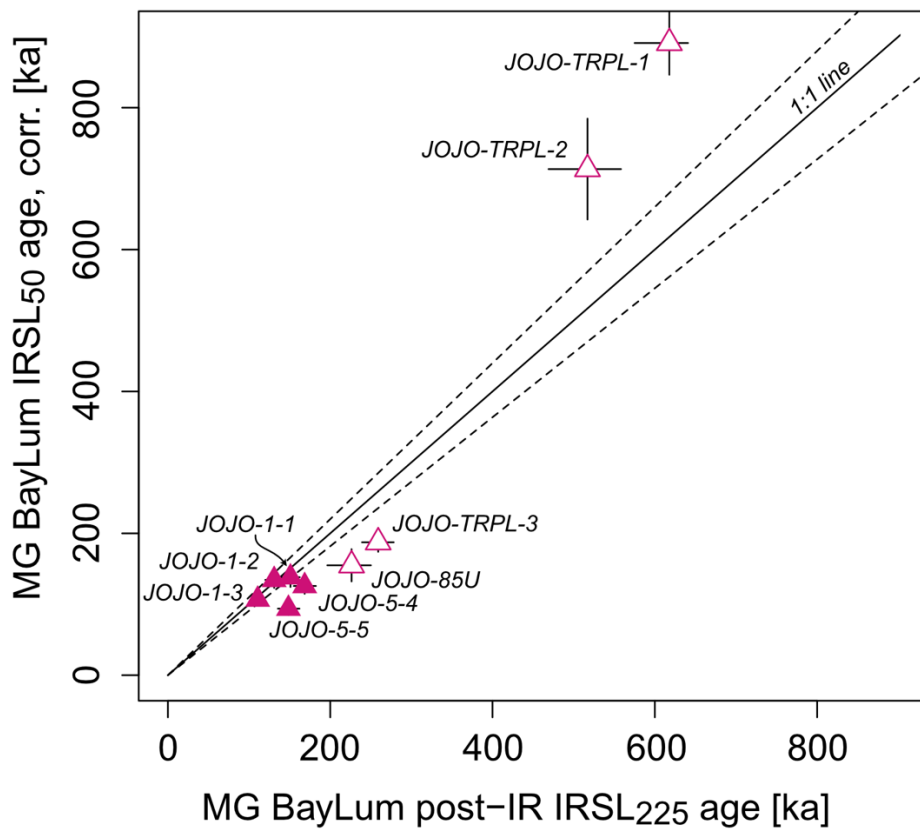


Fig. S10. Comparison of multi-grain aliquots post-IR IRSL₂₂₅ ages and multi-grain fading corrected IRSL₅₀ ages (site-specific average used for correction, see main text). The younger samples with equivalent doses within the linear part of the dose response curve are shown as filled symbols, open symbols represent samples with D_e values not within the linear part of the dose response curve. Fading correction followed Huntley and Lamothe (2001), which is valid for corrections within the linear part of the dose response curve.

S2.2.3 Standardised growth curve (SGC)

Standardised growth curves (SGCs) were established to be able to use the CAM (as representation of the frequentist approaches) for data sets containing saturated grains or multi-grain aliquots.

For this the data stored in .binx files was re-analysed using numOSL (Peng et al., 2017). The acceptance criteria defined in the main text were used. Since the created SGC was of insufficient quality, two further acceptance criteria were added: reduced chi square and figure of merit. This reduced the number of accepted grains/MG aliquots but ensured a qualitatively sufficient SGC to be established. Two SGCs were created in this study: One for the single grain and one for the 1 mm aliquot data. In the least-squares (LS) normalisation procedure contained in the numOSL::lsNORM() function, dose response curves of the accepted grains or aliquots were iteratively rescaled until all MG aliquots or grains converged to one dose response curve (i.e., the SGC) described by a single saturation exponential function. All regenerative cycles in the SAR protocol were used for the LS-normalisation and the same scaling factor obtained for the L_x/T_x values was used to renormalise the corresponding L_n/T_n values. Only data from this study was used for the SGCs and the same grains/multi-grain aliquots were used to establish the SGC and to interpolate renormalised L_n/T_n values onto the SGC. Thus, the SGC was used only to allow for the application of the L_nT_n method to avoid the D_e underestimation caused by grains near signal saturation and not for the reduction of measurement time. Figures S11 and S12 show the dose response curves before and after the LS-normalisation for the single grain and multi-grain aliquot data sets, respectively.

Since we are particularly interested in including saturated and uncertainty saturated grains/aliquots in our palaeodose calculations, we here only consider the SGC L_nT_n method (Li et al., 2017, 2020). Figure S13 shows the single grain SGC results in comparison to the single grain standard CAM (Fig. S13a) results, and the single grain BayLum results (Fig. S13b). Fig. S13c compares the multi-grain SGC L_nT_n results to the multi-grain BayLum results. Finally, Fig. S13d shows a good agreement between the SGC L_nT_n results measured for single grains and multi-grain aliquots.

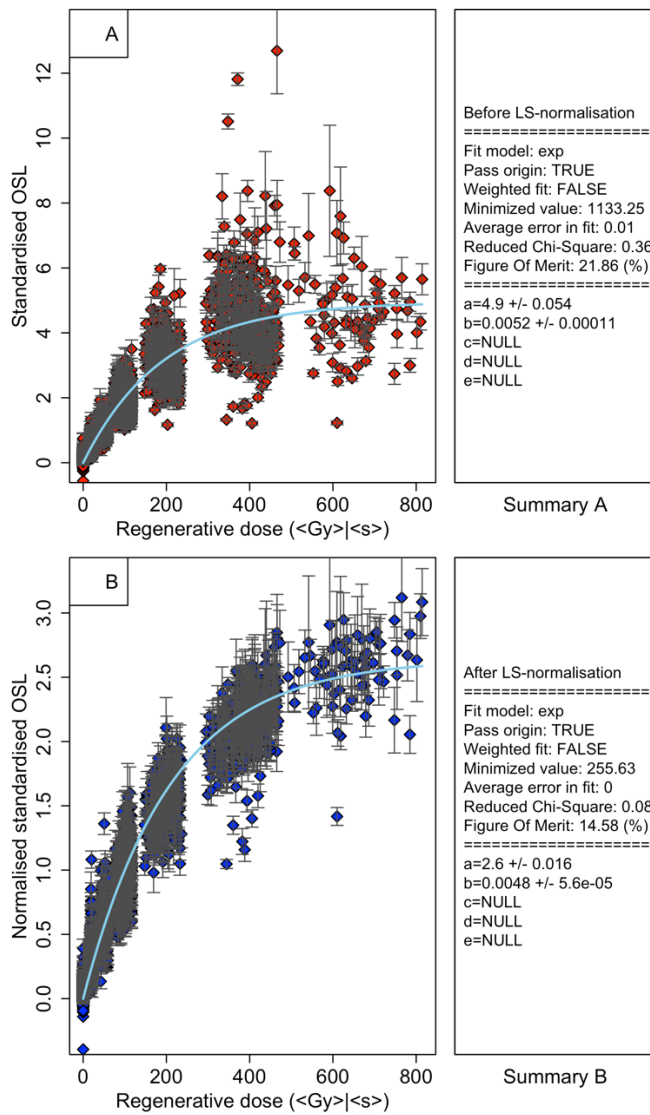


Fig. S11. Least-square normalisation of dose response curves for single grains. (a) Before LS-normalisation, (b) after LS-normalisation. The x-axis unit is Gy.

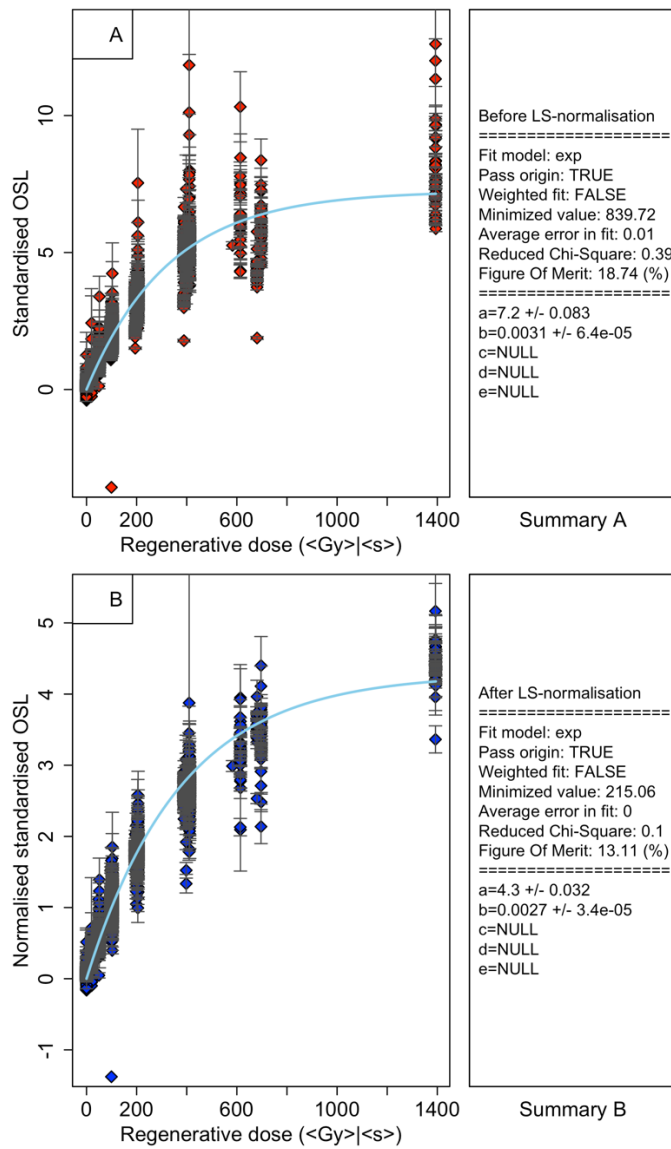


Fig. S12. Least-square normalisation of dose response curves for 1 mm aliquots. (a) Before LS-normalisation, (b) after LS-normalisation. The x-axis unit is Gy.

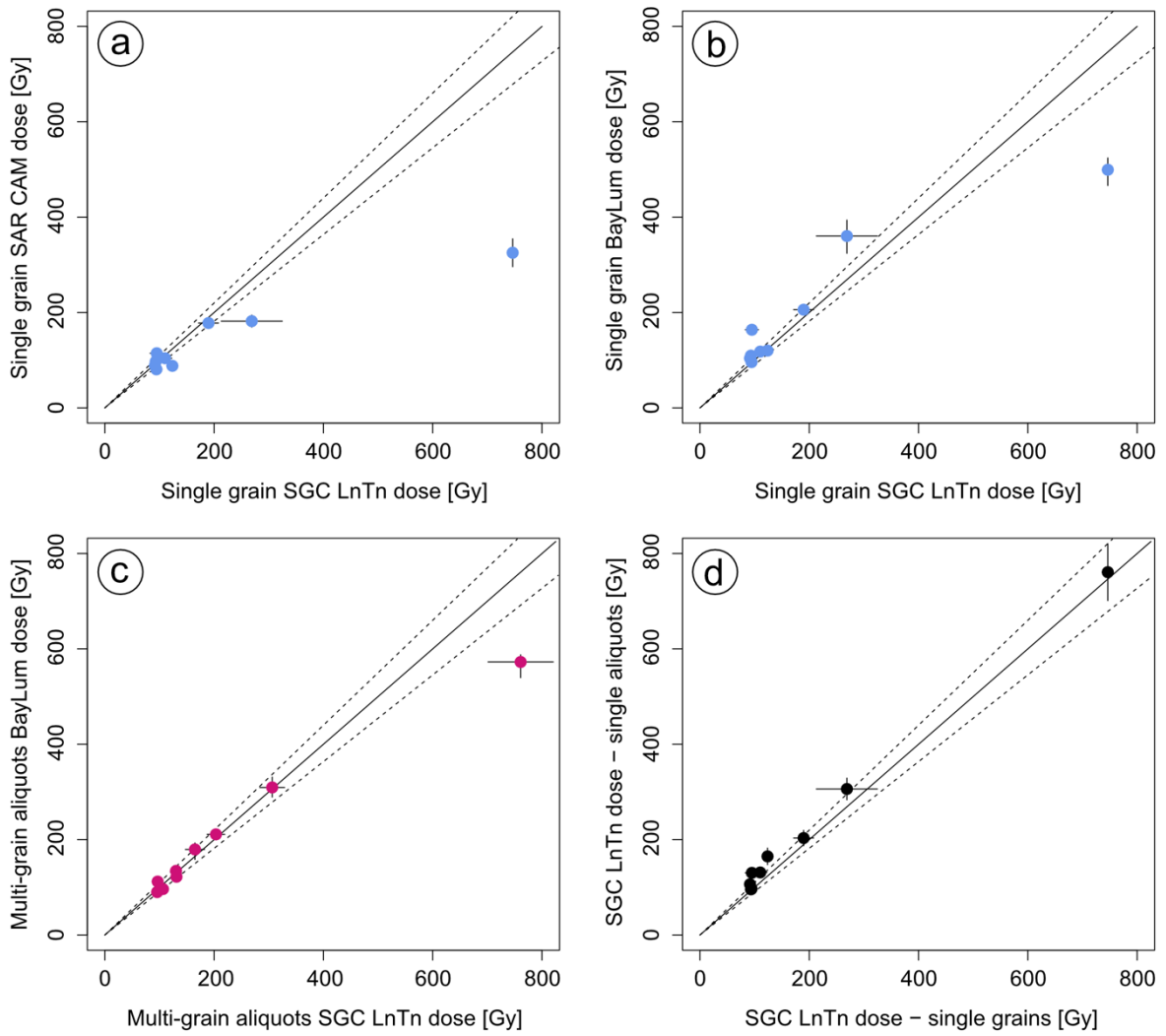


Fig. S13. Evaluation of the SGC L_nT_n approach compared to (A) standard CAM, and (B) single grain BayLum. (C) Evaluation of the SGC L_nT_n approach for single grains and multi-grain aliquots and (D) single grain SGC L_nT_n compared to multi-grain aliquots L_nT_n .

References

Burow, C.: `calc_CentralDose()`: Apply the central age model (CAM) after Galbraith et al. (1999) to a given De distribution, Function version 1.4.1, In: Kreutzer, S., Burow, C., Dietze, M., Fuchs, M.C., Schmidt, C., Fischer, M., Friedrich, J., Mercier, N., Philippe, A., Riedesel, S., Autzen, M., Mittelstrass, D., Gray, H.J., and Galharret, J.: *Luminescence: Comprehensive Luminescence Dating Data Analysis*, R package version 0.9.23, <https://CRAN.R-project.org/package=Luminescence>, 2023.

Christophe, C., Philippe, A., Kreutzer, S., Guérin, G., and Baumgarten, F.H.: *BayLum: Chronological Bayesian Models Integrating Optically Stimulated*, R package version 0.3.2.9000-34, <https://CRAN.R-project.org/package=BayLum>, 2023.

Christophe, C., Philippe, A., and Kreutzer, S.: `calc_AverageDose()`: Calculate the Average Dose and the dose rate dispersion, Function version 0.1.5, In: Kreutzer, S., Burow, C., Dietze, M., Fuchs, M.C., Schmidt, C., Fischer, M., Friedrich, J., Mercier, N., Philippe, A., Riedesel, S., Autzen, M., Mittelstrass, D., Gray, H.J., and Galharret, J.: *Luminescence: Comprehensive Luminescence Dating Data Analysis*, R package version 0.9.23, <https://CRAN.R-project.org/package=Luminescence>, 2023.

Duller, G.A.T.: The Analyst software package for luminescence data: overview and recent improvements, *Ancient TL*, 33, 35-42, 2015.

Galbraith, R.F., Roberts, R.G., Laslett, G.M., Yoshida, H., and Olley, J.M.: Optical dating of single and multiple grains of quartz from Jinmium rock shelter, Northern Australia: Part I, experimental design and statistical modelling, *Archaeometry*, 41, 339-364, 1999.

Guérin, G., Christophe, C., Philippe, A., Murray, A.S., Thomsen, K.J., Tribolo, C., Urbanova, P., Jain, M., Guibert, P., Mercier, N., Kreutzer, S., and Lahaye, C.: Absorbed dose, equivalent dose, measured dose rates, and implications for OSL age estimates: Introducing the Average Dose Model, *Quat. Geochronol.*, 41, 163-173, doi:10.1016/j.quageo.2017.04.002, 2017.

Huntley, D.J. and Lamothe, M.: Ubiquity of anomalous fading in K-feldspars and the measurement and correction for it in optical dating. *Can. J. Earth Sci.* 38, 1093-1106, doi: 10.1139/cjes-38-7-1093, 2001.

Kreutzer, S., Burow, C., Dietze, M., Fuchs, M.C., Schmidt, C., Fischer, M., Friedrich, J., Mercier, N., Philippe, A., Riedesel, S., Autzen, M., Mittelstrass, D., Gray, H.J., and Galharret, J.: *Luminescence: Comprehensive Luminescence Dating Data Analysis*, R package version 0.9.23, <https://CRAN.R-project.org/package=Luminescence>, 2023.

Peng, J., Li, B., More, J., Garbow, B., Hillstrom, K., Burkardt, J., Gilbert, P., and Varadhan, R.: numOSL: Numeric Routines for Optically Stimulated Luminescence Dating, <https://cran.r-project.org/package=numOSL>, 2017.

Philippe, A., Guerin, G., and Kreutzer, S.: BayLum – An R package for Bayesian analysis of OSL ages: An introduction. *Quat. Geochronol.* 49, 16-24, doi: 10.1016/j.quageo.2018.05.009, 2019.